

Turbulent Flow-Driven Molecular Cloud Formation: A Solution to the Post-T Tauri Problem?

Javier Ballesteros-Paredes^{1,2}, Lee Hartmann², and Enrique Vázquez-Semadeni¹

¹Instituto de Astronomía, Universidad Nacional Autónoma de México

Apdo. Postal 70-264, 04510 México D.F., México. e-mail: javier@astrocu.unam.mx

²Harvard-Smithsonian Center for Astrophysics, 60 Garden St., MS-42, Cambridge MA 02138

ABSTRACT

We suggest that molecular clouds can be formed on short time scales by compressions from large scale streams in the interstellar medium (ISM). In particular, we argue that the Taurus-Auriga complex, with filaments of $10\text{-}20\text{ pc} \times 2\text{-}5\text{ pc}$, most have been formed by H I flows in $\lesssim 3\text{ Myr}$, explaining the absence of post-T Tauri stars in the region with ages $\gtrsim 3\text{ Myr}$. Observations in the 21 cm line of the H I “halos” around the Taurus molecular gas show many features (broad asymmetric profiles, velocity shifts of H I relative to ^{12}CO) predicted by our MHD numerical simulations, in which large-scale H I streams collide to produce dense filamentary structures. This rapid evolution is possible because the H I flows producing and disrupting the cloud have much higher velocities ($5\text{-}10\text{ km s}^{-1}$) than present in the molecular gas resulting from the colliding flows. The simulations suggest that such flows can occur from the global ISM turbulence without requiring a single triggering event such as a SN explosion.

1. Introduction

It has been recognized for many years that the nearest star-forming regions exhibit little evidence for stars of ages $\gtrsim 5\text{ Myr}$, even though one would expect that such “post-T Tauri stars” (PTTSs) should be more numerous than the $\sim 1\text{ Myr}$ -old T Tauri stars. More than a decade ago, Herbig, Vrba, & Rydgren (1986) stated that “it is a source of some unease that this large population of PTTSs has not yet been identified.” Since that time, a variety of techniques have been used to search for PTTSs, including proper motion surveys, fainter objective prism plates, CCD photometric selection. As outlined in §2, none of these techniques has yielded evidence for PTTSs in any significant numbers.

The lack of PTTSs, combined with the presence of newly-formed stars in all substantial nearby molecular clouds, is most simply explained if molecular clouds like Taurus come together, form stars, and disperse in a few Myr. However, this simple picture causes difficulties for current theories of star formation. Since Taurus has a spatial extent of 20 pc , but the molecular gas has a velocity dispersion of only about 2 km s^{-1} , it is difficult to understand how such widely separated regions produced stars almost simultaneously, i.e., how star formation is “triggered” throughout the cloud on a scale shorter than the crossing (or dynamical) timescale. In principle, a single powerful event like a supernova explosion might trigger star formation in a molecular cloud over short timescales, but there is no obvious candidate for this triggering source in the case of Taurus (Elmegreen 1993a).

In addition, Taurus is supposed to be the archetype for the “standard” picture of isolated, low-mass star formation, in which magnetically subcritical cloud cores collapse to form stars only after ambipolar diffusion has removed excess magnetic flux on timescales of order $5\text{-}10\text{ Myr}$ (Shu, Adams, & Lizano 1987; Mouschovias 1991, and references therein). If protostellar cloud cores are highly subcritical, the long

ambipolar diffusion timescale makes it difficult to understand star formation events lasting only a few Myr. A long diffusion time also is difficult to reconcile with statistics of cloud cores (Lee & Myers 1999).

Palla & Galli (1997) argued that the ambipolar diffusion timescale simply introduces an age offset. In this picture, the molecular cloud cores which produced the present-day Taurus stars started contracting, say, 11-12 Myr ago, so that the cores have only become supercritical and started collapsing over the last 1-2 Myr. However, there is no unique ambipolar diffusion timescale; it depends upon the ionization fraction, which in turn depends upon precise conditions of shielding (Myers & Khersonsky 1995), and on how subcritical the cloud core is initially. Thus it is difficult to understand how ambipolar diffusion does not introduce a spread of at least several Myr into the onset of star formation. Moreover, as pointed out by Fiedler & Mouschovias (1993), Nakano (1998), and Hartmann (1998), strongly subcritical clouds must be confined by external pressure to prevent disruption by expansion. The possibility of producing a steady external pressure in the generally turbulent environment of molecular clouds has been questioned recently by Ballesteros-Paredes, Vázquez-Semadeni, & Scalo (1998 = BVS99), who suggest that the turbulent motions are not steady, and can disrupt as well as compress clouds. Given these problems and the evidence of the stellar population, it appears likely that ambipolar diffusion is not a major constraint on the timescale of star formation in Taurus, as argued by Nakano (1998) on general grounds, and as proposed many years ago by Shu, Adams, & Lizano (1987) for much denser regions.

Even if the ambipolar diffusion timescale is not relevant, there still remains the problem of triggering star formation in Taurus. This is possible in a dynamical scheme, where large-scale turbulent streams collide, collecting the material they are advecting and creating density fluctuations (Hunter 1979; Hunter & Fleck 1982; Hunter et al. 1986; Tohline et al. 1988; Elmegreen 1993b; Vázquez-Semadeni, Passot & Pouquet 1995 = VPP95; BVS99; see also Vázquez-Semadeni et al. 1999). In this picture the formation of molecular clouds cannot be considered separately from the formation of their parent diffuse H I clouds. If molecular gas clouds like Taurus are “assembled” by the convergence of higher-velocity neutral hydrogen flows, one might explain the nearly-simultaneous star formation over larger distance scales without invoking a single triggering event, like a SN explosion.

In this paper we consider the dynamical, kinematic and spatial relationship between the neutral hydrogen and molecular gas in the Taurus region. Our analysis is based on H I and ^{12}CO observations, showing that in many places there is H I which appears to be dynamically correlated with the molecular gas, but with substantial velocity offsets and larger velocity dispersions. The dynamical timescales for the clouds are then given by the scale of the clouds divided by the velocity dispersion of the external H I, contrary to the assumption that the internal velocity dispersion is the relevant quantity. We further show that these results are qualitatively consistent with MHD simulations of the ISM, suggesting that the molecular clouds like Taurus can be rapidly assembled, eliminating the need to find PTTSs in the present molecular gas complex.

In §2 we review the observations leading to the post T-Tauri problem. In §3 we explore the dynamical relationship between H I and CO gas in the Taurus region, while in §4 we show simulations of the ISM dynamics which we use to interpret the observations in §5.1. Finally, we point out limitations of our simulations in §5.2, and summarize our conclusions in §6.

2. Historical Context: The post-T Tauri problem

Analyses of molecular cloud lifetimes have rarely included constraints from their stellar populations; yet the ages of the stars produced by these clouds provide uniquely detailed constraints on cloud ages that are not obtainable in any other way (e.g., Hartmann et al. 1991; Feigelson 1996). Because of the importance of the stellar population ages, it is worth reviewing the situation in some detail, especially given some of the conflicting literature on the subject. We focus on the Taurus-Auriga molecular cloud complex, where the most detailed observational efforts have been made.

To illustrate the problem, Figure 1 a shows the HR diagram for stars in the Taurus-Auriga molecular cloud region, with stellar luminosities and effective temperatures taken from Kenyon & Hartmann (1995). The great majority of the stars have ages near 1 Myr; approximately half are younger than this, while only a few stars have ages greater than 3 Myr (see Fig 1 b).

The group of stars near the 100 Myr isochrone (i.e., near the zero-age main sequence) were discovered through early *Einstein* X-ray surveys (Walter et al. 1988, and references therein). These stars were originally suggested by Walter et al. (1988) as members of the missing PTTs population. However, there is a striking gap in the HR diagram; there are very few stars filling in the age range between ~ 5 and 50 Myr. This gap makes it very unlikely that a single, reasonably continuous star formation event is responsible for both the near-ZAMS stars and the young T Tauri stars. Furthermore, with such large ages it is difficult to connect these stars with the present Taurus molecular cloud. Walter et al. (1988) found ages for these stars ~ 30 Myr at a modest velocity dispersion of 2 km s^{-1} , typical of Taurus molecular gas. These stars can have traveled 60 pc from their birth-sites during their lifetimes, 3 times the diameter of the Taurus molecular complex.

The apparent coordination of star formation on relatively short timescales in Taurus (and other regions) has led to several efforts to identify hypothetical older stars which might be present but missed in previous objective prism surveys dependent upon strong $H\alpha$ emission. Herbig, Vrba, & Rydgren (1986) obtained objective prism data covering the Ca II H and K emission lines, which are present in much older stars. Indeed, Herbig et al. (1986) identified several outlying members of the Hyades in their survey (see also Hartmann, Soderblom, & Stauffer 1987), but failed to identify any older PTTs. Hartmann et al. (1991) and Gomez et al. (1992) used proper-motion surveys to try to select members of Taurus without regard to emission line properties; again, no substantially older stars were found.

It has been suggested that recent X-ray surveys (e.g., Walter et al. 1988; Neuhäuser et al. 1995; Wichmann et al. 1996) have discovered the missing PTTs. However, the ages of the typical G and early K stars in these samples are uncertain, because neither X-ray activity nor Li depletion clearly discriminate between 1 Myr-old T Tauri stars and 100 Myr-old stars. It seems likely that most of these objects are 30-100 Myr-old stars, given their numbers and properties (Briceño et al. 1997). More recent measurements of Li depletion (Martin & Magazzu 1998) and limits on the M star component of the G-K ROSAT survey population (Briceño et al. 1998) support the idea that most of the dispersed X-ray population is much older than 10 Myr. Indeed, it is difficult to explain the spatial distributions of these stars if they are much younger. The dispersed X-ray sources are spread fairly uniformly over large distances (up to 70 pc in projected distance from the center of Taurus); it would be very difficult to move stars from the present molecular regions this far at typical velocity dispersions of $\sim 2 \text{ km s}^{-1}$ in anything less than about 30 Myr. Instead, it seems much more likely that these stars are mostly ~ 50 Myr-old objects which formed in a variety of individual regions whose molecular gas has by now dispersed (Feigelson 1996). Whatever the exact age of the Einstein- and ROSAT-discovered young stars, they do not seem to represent the “missing”

stars in Taurus of ages 3-10 Myr.

Another approach has been to consider whether the ages of the Taurus stars have been systematically underestimated. For example, the evolutionary tracks of Swenson et al. (1994) give ages for Taurus stars that would be several times larger than those of D’Antona & Mazzitelli (1994), which were used in Figure 1. However, as pointed out by Stauffer et al. (1995), if one modifies the calibrations of evolutionary tracks so that the calculations match the zero-age main sequence, most of the age discrepancy between those works disappears. Another possibility was raised by Hartmann & Kenyon (1990), who suggested that the effects of accretion might produce spurious age estimates, but more recent investigations (Hartmann, Cassen, & Kenyon 1997; Siess, Forestini, & Bertout 1997) indicate that T Tauri accretion has little effect, making the stars appear slightly older, not younger. One may also note (Mizuno et al. 1995) that most of the pre-main sequence stars in Taurus lie within 1-2 pc of dense molecular gas; at a velocity of 1-2 km s⁻¹, this suggests that these stars have not been dispersing for more than 1-2 Myr from their natal material, in agreement with the conventional HR diagram ages.

Thus, all the Taurus observational constraints are consistent with a picture in which the molecular gas comes together and forms stars in $\lesssim 3$ Myr, so that few stars of ages 3-10 Myr are expected. The widely-distributed X-ray sources mostly represent stars which, though relatively young, are generally substantially older than 10 Myr, and it is likely that their natal molecular clouds no longer exist.

A general absence of PTTs implies not only that clouds form stars rapidly, but that star-formation timescales are also relatively short. Since Taurus is still forming stars, its ultimate dispersal time is not known. However, studies of other regions such as Cha I and IC 348 (Lawson et al. 1996; Herbig 1998) provide relatively little evidence for large populations of PTTs, especially when older ROSAT sources are eliminated and mass-dependent biases are eliminated.¹ From the absence of known molecular cloud regions containing 10 Myr-old stars, it appears that the molecular gas may also disperse in a few Myr, a timescale consistent with the cluster survey results of Leisawitz, Bash, & Thaddeus (1989). In this picture many molecular clouds will not have substantial populations of PTTs.

3. Atomic and molecular gas: Maps and velocity-position diagrams

The Taurus clouds are well-suited for understanding gas dynamics as well as the stellar population. The Taurus Molecular Cloud (TMC) is one of the most well-studied molecular clouds in the sky, with extensive H I and CO maps; it is one of the nearest clouds and lies well below the galactic plane, making it easier to isolate the H I associated with the CO cloud from the general material in the galactic plane. Finally, the morphology and kinematics of TMC suggests a close relationship between the molecular and atomic gas (see PhD thesis and series of papers by Andersson 1993, and references therein).

In the following discussion we make use of both H I and ¹²CO data. The 21 cm line data were taken from the Atlas of Galactic Neutral Hydrogen (Hartmann & Burton 1997) obtained with the 25 m Leiden/Dwingeloo telescope, while the ¹²CO molecular data have been taken from Ungerechts & Thaddeus (1987), obtained with the Columbia millimeter-wave telescope. Details of the observations and analysis may be found in the original papers. Here we note that both data sets have 0.5 degree spatial resolution, which facilitates comparison. The velocity resolution of the H I data is 1.03 km s⁻¹, slightly lower than that of

¹Age estimates for cluster stars generally depend systematically on stellar mass, probably due to birth-line errors (i.e., uncertainty in the initial positions of protostars in the HR diagram; Hillenbrand 1997; Hartmann 1999.)

the CO data, 0.65 km s^{-1} . To overlap the ^{12}CO and atomic maps, we transformed the molecular data set (originally in (RA,DEC)) to galactic coordinates (l, b) by triangulating and re-sampling the transformed data in a half degree resolution grid. We present both sets of data extending from 140 to 201 degrees in galactic longitude, and from -44 to $+17$ in galactic latitude (note that the original ^{12}CO data does not cover the whole range. We only add zeros in the external region, in order to match the H I and ^{12}CO data at large scales).

Figure 2 shows a velocity-integrated map in ^{12}CO (isocontours) and H I (gray-scale) for the velocity range where the CO data has been obtained ($-20.33 \text{ km s}^{-1} \leq v_{\text{LSR}} \leq 29.1 \text{ km s}^{-1}$). The straight lines indicate the loci of the cuts along which the velocity-position diagrams shown in Figure 3 are made. Assuming an optically thin medium, the H I intensity (in K km s^{-1}) can be considered as proportional to the column density with a conversion factor of $1.8 \times 10^{18} \text{ cm}^{-2}$. The gray scale range in Figure 2 corresponds to a column density range from $\sim 2.5 \times 10^{20} \text{ cm}^{-2}$ (darker pixels), to a few times 10^{21} cm^{-2} (white pixels). A column density of 10^{21} cm^{-2} , corresponding to $A_V \sim 0.5$, is generally taken to be roughly the minimum column density needed for sufficient shielding of the UV radiation field to produce CO (e.g., Elmegreen 1993a).

In Figure 3 we present a set of six velocity-position diagrams for both the H I and ^{12}CO emission. The first two panels (cuts 1 and 2 in Fig. 2) are the velocity-position diagrams for the region that formally is known as TMC, in which ^{13}CO has been detected (see e.g. Kleiner & Dickman 1984; Mizuno et al. 1995; etc.). Figure 3 c (cut 3) corresponds to the region associated with Perseus Arm, and shows a strong velocity gradient, from $\sim 8\text{-}10 \text{ km s}^{-1}$ to $\sim -2 \text{ km s}^{-1}$. Figure 3 d (cut 4) corresponds to the northernmost region mapped by Ungerechts & Thaddeus (1987). In Figure 3 e (cut 5) we present a velocity-position diagram that covers a large region, going from high southern latitudes to close to the galactic plane. Finally, in Figure 3 f (cut 6) we show the velocity-position diagram for the nearby cloud L1457. In particular, note from Figure 3d and e that at low galactic latitudes the H I exhibits a large velocity spread due to the detection of material at a wide range of distances in the galactic plane. However, once one moves out of the plane a sufficient distance ($b < -10^\circ$), the H I velocity width becomes substantially smaller. The H I velocity peak is generally fairly close to, although not identical with, the ^{12}CO peak. This reflects the fact that the ^{12}CO and H I emission are spatially and kinematically related, suggesting that they are produced as part of a single dynamical complex (see, e.g., Blitz & Thaddeus 1980).

From Figure 3 the following features can be noted. First, wherever there is a ^{12}CO feature, H I is also found, with an approximate column density similar to that required by shielding (see above). Second, the converse is not true: not all H I in this velocity system is associated with molecular gas. Third, at a given spatial position, the H I emission often does not peak at the same velocity than the ^{12}CO ; frequently there is an offset of a few km s^{-1} between the two species. Fourth, velocity widths in the H I spectra are larger than the ^{12}CO spectra by a factor of roughly 3 or more. Fifth, both the ^{12}CO and H I line profiles are asymmetric, as indicated by the variation of gray-scale and contours in Figure 3a-l. These characteristics have been noticed previously in other regions (see e.g., Blitz & Thaddeus 1980; Magnani, Blitz & Mundy 1985; Elmegreen & Elmegreen 1987), and we shall focus on these properties when comparing with numerical simulations in the next section.

4. NUMERICAL SIMULATIONS

4.1. The Model

To interpret the significance of the observed features of the atomic and molecular gas enumerated at the end of §3, we turn to numerical simulations of the interstellar medium by Passot, Vázquez-Semadeni, & Pouquet (1995 = PVP95). These two-dimensional simulations represent the behavior of a one square kiloparsec of the ISM centered at the solar galactocentric distance. The simulations solve the MHD equations, including self-gravity, parameterized cooling and diffuse heating, the Coriolis force, large-scale shear, and parameterized localized stellar energy input due to ionization heating. The parameterized cooling is as in Chiang & Bregman (1988), who fitted piecewise power laws to the standard cooling calculations of Dalgarno & McCray (1972) and Raymond, Cox & Smith (1976) (see Vázquez-Semadeni, Passot, & Pouquet 1996 = VPP96 for details). As discussed in VPP96, the cooling and diffuse heating time scales are in general much shorter than the dynamical time scales, implying that the flow is always in thermal equilibrium, except in the vicinity of star formation sites. We refer to the reader to VPP96 for further details in the equations and the model itself, and to the video accompanying PVP95, which gives an animated view of the dynamics of the ISM and shows the transient character of the clouds².

Because the present MHD simulations do not include chemistry, we adopt a picture in which molecular clouds are the “tips of the icebergs” of the density features in the simulations. We define a ‘molecular’ cloud as a connected set of pixels with density above some density threshold ρ_{th} . The selection of this density threshold is arbitrary, but it must be a compromise between realistic values for molecular clouds and the limitations of the simulations. Because the densest and smallest structures in the simulations reach values $\rho \sim 50 - 100 \text{ cm}^{-3}$, we select a density threshold of 35 cm^{-3} , unless otherwise stated. For comparison, typical mean densities in molecular clouds start at roughly 20 cm^{-3} (e.g., Blitz 1987). In particular, an average value of 15 cm^{-3} is reported for Rosette Molecular cloud (Williams, Blitz & Stark 95).

The simulations have a mean density of $\langle n \rangle = 1 \text{ cm}^{-3}$, which corresponds to a mean column density of $\langle N \rangle \sim 3.1 \times 10^{21} \text{ cm}^{-2}$ integrating through the 1 kpc box. This value is large enough to envision enough shielding to UV radiation to form molecular hydrogen (see e.g. Franco & Cox 1986).

For the analysis here, we use a run presented in Ballesteros-Paredes, Vázquez-Semadeni & Rodríguez (1997 = VBR97) called run 28.800, which has a resolution of 800×800 pixels. In order to mimic as much as possible the conditions in Taurus, we turn off the star formation at $t = 68.9 \text{ Myr}$ (5.3 code units). This allows us to increase the density contrasts, and to avoid the heating from massive stars, which are not present in Taurus. Then, we follow the time evolution of a relatively small cloud, which is localized far away from the big cloud complexes formed in the simulations.

4.2. Results

In Figure 4 we show a time-sequence of a subsection of the whole box of the simulation, starting 7.02 Myr after the time in which we turn off the star formation. The grey scale indicates the density field, ranging from 0.31 to 56.6 cm^{-3} , and arrows denote the velocity field in the reference frame of the cloud. The snapshots are separated by $\Delta t = 0.39 \text{ Myr}$ (0.03 time code units). The black isocontour is the region where the density values are higher than 35 cm^{-3} . Note that the cloud is located where the velocity field converges, as required by the continuity equation. Also, one observes rapid growth (within less than 2 Myr)

²See also <http://www.astroscu.unam.mx/turbulence/movies.html>

of a “cloud” above our density threshold which is approximately 20 pc in length (each pixel unit is 1.25 pc), comparable to the length of the main Taurus clouds.

To show that the density features observed in the simulations are produced by the confluence of external large-scale streams³ rather than other way around (e.g., the velocities being the consequence of, say, gravitational collapse of the cloud), we calculate the time evolution of both characteristic lengths and energies for the density features in Fig. 4. We select a connected set of pixels with densities equal or higher than the half value of the maximum density at each timestep to calculate properties for the “cloud”, a choice motivated by the fact that the maximum density in the box is changing substantially during the simulation (from ~ 16 to $\sim 60 \text{ cm}^{-3}$).

In Fig. 5 we display the evolution of two different characteristic lengths: a) l_x , the maximum x -length of the cloud (solid line); and b) l_J , the Jeans length (dotted line) calculated as

$$l_J = \left[\frac{\gamma_{\text{eff}} \pi c_i^2}{G \rho_0^{2-\gamma_{\text{eff}}}} \right]^{1/2}, \quad (1)$$

where γ_{eff} is the effective polytropic index in the simulations resulting from equilibrium between the heating and cooling rates, c_i is the isothermal speed of sound, and ρ_0 is the mean density of the cloud (see VPP96 for details). The values of these lengths are denoted on the left-hand side y -axis. We also display the evolution of three different energies: a) the absolute value of the gravitational energy $E_{\text{grav}} = -1/2 \int \rho \phi dV$ (short-dashed line), where ρ is the density and ϕ is the gravitational potential; b) the kinetic energy in the frame of the cloud $E_{\text{kin,cloud}} = 1/2 \int_V \rho (\mathbf{u} - \mathbf{u}_{\text{mass}})^2 dV$ (long-dashed line), where \mathbf{u} is the velocity field and \mathbf{u}_{mass} is the mass-weighted average velocity of the cloud; and c) the magnetic energy $E_{\text{mag}} = 1/8\pi \int_V B^2 dV$ (dot-dashed line), where \mathbf{B} is the magnetic field. Note that in all the previous integrals, the volume element is $dv = dx dy$, because of the two-dimensional character of the simulations and thus all the energies considered here are strictly per unit length in the z -direction. The values of the energies are denoted in the left-hand side of the y -axis. The x -axis runs from $t = 0$, the timestep when we turned off the star-formation in the simulations, to 15.2 Myrs after.

At $t = 0$ the Jeans length (dotted line) is initially larger than the x -length l_x (solid line) (the difference was larger at earlier times). This comparison suggests that, at least in this direction, the density structure is not formed by gravitational collapse. We have calculated also the Jeans-length for the whole subregion (not showed here), and find that it is again larger than the length of the subregion size. These results suggest that even if the region must ‘feel’ the action of the gravity, it is Jeans stable at the beginning, and that the velocity field is mostly the result of the global dynamics of the turbulent flow, not the central gravitational action.

As a result of the overall flow, the (2D) “filament” that first appears merges with another structure at $t \sim 8 \text{ Myr}$ (see Fig. 4). This results in the jump in properties seen in Fig. 4, except for l_J , which depends on intensive quantities: the mean temperature and mean density. Independent of this merging, at this time $l_J \sim l_x$, suggesting that now the growth of the cloud is also affected by the gravitational field.

Concerning the time evolution of the energies, it can be seen that the absolute value of the gravitational energy (long-dashed line) is higher than the magnetic energy (dotted-dashed line) by at least two orders of magnitude. This indicates that the cloud is supercritical by a large margin. Furthermore, it can also be seen that the kinetic energy can not be an agent to stop the collapse: besides being smaller than $|E_{\text{grav}}|$ the

³By large-scale streams we refer to random motions whose scales are comparable with the scales of the observed structures.

velocity field is convergent, implying that it is not working against gravity.

Finally, we want to stress that the region called the “molecular cloud” (black isocontour at $\rho_{\text{th}} = 35 \text{ cm}^{-3}$ in Figure 4) appears at roughly the same time in which the region has similar physical and Jeans lengths, i.e., $l_x \sim l_J$, indicating that the value selected of 35 cm^{-3} is reasonably indicative of the time at which the cloud becomes self-gravitating.

As a corollary of the fact that the velocity field is not due to the gravitational potential of the cloud, self-gravitating clouds like that shown in Figure 4 can therefore be produced by the turbulent velocity field, out of an initially stable medium.

How fast these “molecular clouds” can be produced by the general turbulence must depend on how much mass the streams are carrying, how strong the compression is, the rate of cooling of the compressed (shocked) region, the geometry of the compression, etc. For example, the diffuse structure that it is present when we turned off the star formation spends $\sim 7 \text{ Myr}$ to become self gravitant. Nevertheless, Figure 4 shows that in the simulations, self-gravitating structures of 10-20 pc can be coherently formed within a few Myr by this mechanism. Since the densities and velocities in the simulations are realistic, this is a plausible mechanism for molecular cloud formation in the ISM.

4.3. Comparison with Observations

In order to test how the simulations compare with observations, we construct “spectra” for both the densest regions ($\rho \geq \rho_{\text{th}}$, which we call “molecular cloud”) and for the low-density regions ($\rho < \rho_{\text{th}}$, which we call “atomic clouds”). Those spectra are constructed as the mass-weighted velocity (x-component) histograms, mimicking the emission of an optically thin line observed from the left hand side of the box, with a spatial resolution of 1.25 pc (1 pixel), and an ideal telescope. With this approximation, we are implying that the observed ^{12}CO and H I line profiles are good representations of the (mass-weighted) line of sight-velocity field. Also, we are assuming that the ^{12}CO and H I emission do not coexist, which is not necessarily true.

With those spectra (mass-weighted velocity histograms) it is possible to construct a velocity-position diagram, and compare it with the those in Fig 3. Figure 6 is the corresponding velocity-position diagram for the cloud and its surrounding medium shown in Figure 4i. We emphasize several points of similarity between this synthetic position-velocity diagram and the observations (see figure 3). First, the synthetic CO emission is always located within a region of strong synthetic H I emission; second, there are regions where synthetic H I emission is present, but where synthetic ^{12}CO emission is not; third, the maximum of the high-density emission does not necessarily coincide with maximum of the low-density emission; fourth, the velocity dispersion is higher for the synthetic H I emission than from the synthetic ^{12}CO emission, and the velocity dispersions of both the low-density and in the high density gas “emission” have similar line-widths to those of the observational data. Fifth, both ^{12}CO and H I line profiles are asymmetric. Finally, as in the case of Taurus, the filament is almost coherent in velocity dispersion, i.e., it has approximately the same velocity dispersion along itself, with values of $\sim 2 \text{ km s}^{-1}$ along 10-20 parsecs. We will discuss this in §5.1.

5. DISCUSSION

5.1. Evidence for Turbulent Compressions

It is frequently assumed that the ISM is permeated by small-scale non-thermal motions that maintain clouds in a stationary state. Collapse is prevented by those motions, and the role of the external “intercloud” medium is only as an agent for (thermal) pressure confinement and as a shielding for the UV radiation. However, the external medium also exerts a dynamical influence on the cloud, compressing and/or disrupting it (Sasao 1973; Hunter 1979; Hunter & Fleck 1982; Hunter et al. 1986; Tohline et al. 1988; VPP96 BVS99). In this sense, the fragmented appearance of clouds and the existence of multiple velocity components observed at high velocity resolution suggest that cloud’s internal velocity field possesses a disordered or turbulent component at scales comparable with the scales of the clouds. If molecular clouds are embedded in an intercloud medium of atomic hydrogen (see series of papers by Andersson 1993 and references therein), and if the intercloud medium is highly turbulent (see e.g. Braun 1999), it is plausible that molecular clouds and their surrounding gas are in a dynamical state.

Based on refinements of the ISM simulations by PVP95, BVS99 consider the turbulent pressure at cloud “boundaries”. They show that this boundary pressure is generally anisotropic, which distorts the cloud because the energy involved is generally comparable to the internal cloud kinetic energy. In their picture, turbulent motions are not only responsible for cloud support, as is widely accepted: they may also be responsible through large-scale modes of the external turbulence, for shaping and compressing the cloud, possibly even initiating collapse.

In §3 we have shown that line-profiles are asymmetric and show important substructure, features which have been increasingly noticed in high spectral and spatial resolution observations (e.g., Falgarone et al. 1998). These features have been proposed as indicative of large-scale turbulent motions, which may be shaping, distorting and disrupting the cloud (BVS99).

According to the scenario presented here, the observations, which are also reproduced in the simulations, may be interpreted as follows. First, because collisions between H I streams produce the higher density gas (and for reasons of shielding), there should always be H I spatially correlated with molecular gas. Second, the larger velocity dispersion of the H I gas is interpreted as a consequence of its larger spatial extension, and the compression (shocks) and consequent kinetic energy dissipation which occurs when the H I streams collide to form the cloud. Finally, because it is the convergence of macro-turbulent H I streams that produce the high-density material (see Elmegreen 1996), the H I line profiles should be asymmetric and frequently shifted in velocity with respect to the molecular gas⁴.

Thus, the breadth and asymmetry of the H I line profiles indicate a macroscopically-turbulent medium in which clouds exchange mass, momentum and energy with their surroundings. Note that the picture outlined here does not require a coherent or single triggering event in which atomic gas pushes molecular gas together as in a SN explosion. Our scenario is more general, reflecting statistical fluctuations resulting from the combined effects of differing sites.

⁴Note that in a laminar 2-streams collision producing a shock-bounded slab, the optically thin line-profile from the ‘external’ medium must be a double peaked line, at velocities $-v$ and $+v$, where $2v$ is the velocity difference between the streams. On the other hand, the line-profile from the compressed region must be a single peaked line at zero velocity. Nevertheless, in a turbulent medium, with density and velocity fluctuations over the some mean density and velocity profiles increasing at the center of the compressed region, the double peaked line-profile might become a single broader line-profile (with its substructure) enveloping the narrower line-profile that comes from the compressed region, as its observed from the synthetic line-profiles and as it is suggested from the observed line-profiles.

Recognition of these features is not new. The correspondence between H I and CO in position-velocity diagrams has already been noted by several authors (e.g. Blitz & Thaddeus 1980; Elmegreen & Elmegreen 1987; see also Blitz 1987; and references therein). Andersson (1993 and references therein), who observed the spatial transition between molecular and atomic gas in 62 edges in 14 clouds, found all five observational features that we described at the end of §3 and §4.3. Moriarty-Schieven, Andersson & Wannier (1997) suggested that there is morphological evidence that nearby clouds (L 1457, see cut 6 in Figs. 2 and 3 f) have suffered compressions at scales similar to the scales of the cloud. These authors proposed an unobserved SN explosion as a possible mechanism of producing this morphology. However, the observed morphology is hard to reconcile with a single point source of compression, while it is fully consistent with our scenario. Furthermore, the existence of multi-peak, asymmetric line-profiles at all scales (for larger, see e.g., Mizuno et al. 1995; for smaller, see e.g., Falgarone et al. 1998) strongly suggests the multi-scale nature of the turbulent motions (BVS99). Finally, the velocity-dispersion coherence along large structures have already been seen before both in low-mass clouds (Taurus, Mizuno et al. 1995) as well as in high mass clouds (W51 Carpenter & Sanders 1998).

5.2. Limitations of the Model

One of the most important limitations of these simulations is that the cooling laws and the available resolution limit the simulations to densities $\lesssim 100 \text{ cm}^{-3}$, so that the evolution of higher-density (10^2 or more) structures cannot be followed. This is important, because molecular gas probably cannot be formed sufficiently rapidly within our density range. Characteristic H_2 formation rate on grains are of the order of $\tau^{-1} \sim nR$, where n is the density of atomic hydrogen and R , the rate coefficient, has typical values of the order of $3 \times 10^{-17} \text{ cm}^3 \text{ seg}^{-1}$ (Jura 1975). Then, the typical H_2 formation timescales are given by

$$\left(\frac{\tau_{H_2}}{\text{yr}}\right) \sim 10^6 \left(\frac{n}{10^3 \text{ cm}^{-3}}\right)^{-1}. \quad (2)$$

Thus, at our threshold density of 35 cm^{-3} , the H_2 formation timescale is 30 Myr, uncomfortably long.

The low values of the density reached in the simulations’ clouds are consequence of the spatial resolution and the mass diffusion, which smoothes the strong density gradients (see e.g., VBR97). Nevertheless, we envisage that the clouds simulated here would really collapse to structures of much higher density in even shorter times (for example, at $n \sim 100 \text{ cm}^{-3}$, the free-fall time is approximately 3 Myr), given the strength of the external flows, if we were to use higher spatial resolution. In this way our “molecular gas” above the threshold density merely indicates the approximate location and velocity of the higher-density material which would be formed within it. In the real interstellar gas, there is no barrier to compressing gas in the cloud to typical Taurus densities of the order of 10^3 cm^{-3} so that the molecular gas could be produced as rapidly as the dynamical compression occurs.

On the other hand, regions that we identify with molecular gas are not really isothermal in the simulations, but this is not a reason for concern, since we are not dealing with the internal structure of these clouds which are at the limit of the resolution anyway.

Another limitation of the simulations is that they are two-dimensional calculations which assume no variation of properties perpendicular to the galactic plane. While colliding streams in 2D produce filaments, in 3D they may produce sheets. Nevertheless, the most probable situation is one in which the colliding streams are oblique, such that the region that is compressed is a filament again. Also, inhomogeneities in the

physical properties of the streams (density, temperature, etc.) and a set of instabilities which are produced when streams are colliding may destroy the possible appearance of the sheet. Furthermore, the structure in 3D simulations is still strongly filamentary (see e.g., Ostriker et al. 1998; Padoan & Nordlund 1999; Mac Low 1999; Pichardo et al. 1999). BVS99 discuss other possible differences of 2D and 3D simulations.

Thirdly, the energy input into the ISM is assumed to be from high mass star formation, which seems to be of little relevance to low-mass star forming regions like Taurus. However, the only role of the energy input in the present situation is to produce large-scale flows and turbulence which in turn produce the “molecular cloud”; since the predicted motions agree quite well with the H I data, our approach is justified. Moreover, since the stellar energy input is turned off to follow cloud formation, disruption by local high-mass stars is not an issue.

It should be emphasized that while we are considering the simulations with a view toward understanding the Taurus region, we are not attempting to model the complex in detail, because turbulent flows exhibit a chaotic behavior, i.e., the time histories of arbitrarily close initial conditions diverge exponentially and end up completely different (e.g. Lessieur 1990). Instead, they are only expected to statistically reproduce the dynamical relationship between H I flows and molecular gas in a statistical sense

6. SUMMARY

In this paper we have used H I and ^{12}CO data to show that the dynamical features observed through Taurus can be interpreted as large-scale compressions of the atomic gas producing the molecular gas in timescales of few Myr. Also, we followed the evolution of an small piece of 2D numerical MHD simulations to show how large scale turbulence is able to trigger collapse in density structures that originally are Jeans stable. The timescales for doing this also are few Myr, suggesting that low-density H I streams can be compressing and producing the high density regions in Taurus.

With this picture in mind, we suggest that the Taurus molecular cloud may have formed quite recently (~ 3 Myr ago). This would solve the post T-Tauri problem, suggesting that the very few stars with ages between 5 and 10 Myr in the region might be field stars. We also suggest that the general large-scale interstellar turbulence (in H I) is the mechanism responsible for triggering coherent collapse in regions which apparently are dynamically disconnected.

In this paper we have only considered the timescale of cloud formation, not the timescale of disruption or dissipation. Even with a rapid formation time, if clouds live for 10 Myr or more, at least some complexes should have PTTSs. Thus, our investigation only addresses one-half of the more general post-T Tauri problem. We intend to explore the rate of cloud disruption and dissipation in a future contribution.

The simulations were performed on the Cray Y-MP/4-64 of DGSCA, UNAM. This work has received partial support from grants UNAM/DGAPA IN105295 and UNAM/CRAY SC-008397 to E.V.-S. and a UNAM/DGAPA fellowship to J.B.-P. Cesar & John: discusiones. Ungerechts, datos.

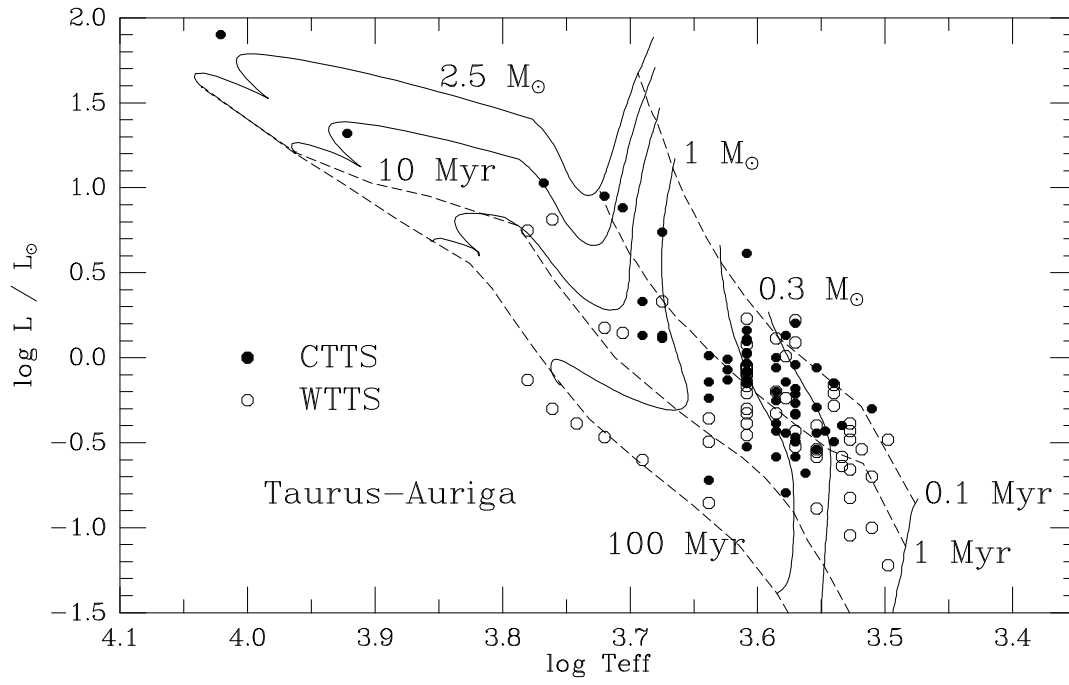
REFERENCES

Andersson, B-G.1993. PhD Thesis. University of Gothenburg, Gothenburg. Sweden

- Ballesteros-Paredes, J., Vázquez-Semadeni, E., & Scalo, J. 1999. ApJ, in press. (VSS99)
- Blitz, L. 1987, in *Physical Processes in Interstellar clouds*, eds. G. E. Morfill, & Scholer, M. (Dordrecht: D. Reidel Publishing Company), p. 35
- Blitz & Thaddeus 1980. ApJ 241, 676
- Braun, 1999. in *Interstellar Turbulence*. Eds. Franco, J. & Carramiñana, A. (Cambridge: University Press), in press.
- Briceño, C., Hartmann, L. W., Stauffer, J. R., Gagné, M., Stern, R. A., & Caillault, J. P. 1997. AJ, 113, 740
- Briceño, C., Hartmann, L. W., Stauffer, J. R., Martín, E. 1997. AJ, 115, 2074
- Briceño, C., Calvet, N., Kenyon, S., & Hartmann, L. 1999. ApJ, accepted
- Carpenter, J. M., & Sanders, D. B. 1998. AJ, 116, 1856
- Chiang, W. H. & Bregman, J. N. 1988. ApJ 328, 427
- Dalgarno A. & McCray, R. A. 1972. ARA& A 10, 375
- D’Antona, F., & Mazzitelli, I. 1994, ApJS, 90, 467
- Elmegreen, 1993a. In *Protostars and Planets III*. Ed. E. H. Levy & J. I. Lunine. (Tucson: Univ. of Arizona Press), p. 97.
- Elmegreen, 1993b. ApJL 419, L29
- Elmegreen, 1996. In *Unsolved Problems of the Milky Way*, ed. L. Blitz and P. Teuben. Kluwer Academic Publishers, p. 551
- Elmegreen, B. G. & Elmegreen D. 1987. ApJ, 320, 182
- Falgarone, E., Panis, J.-F., Heithausen, A., Perault, M., Stutzki, J., Puget, J.-L. & Bensch, F. 1998. *A&A*, 331, 669
- Feigelson, E.D., 1996, ApJ, 468, 306
- Fielder, R. A., & Mouschovias, T. Ch. 1993. ApJ, 415, 680
- Frank, J. J., & Cox, D. P. 1986. PASP, 98, 1076
- Gomezetal92 Gomez, M., Jones, B.F., Hartmann, L., Kenyon, S.J., Stauffer, J.R., Hewett, R., & Reid, I.N. 1992, AJ, 104, 762
- Hartmann, D., & Burton, W. B. 1997. *Atlas of Galactic Neutral Hydrogen*. Cambridge University Press.
- Hartmann, L., 1998, *Accretion Processes in Star Formation*, Cambridge University Press, p. 33
- Hartmann, L., 1999, *New Astronomy Rev.*, in press
- Hartmann, L., Cassen, P., & Kenyon, S.J. 1997, ApJ, 475, 770
- Hartmann, L., & Kenyon, S.J. 1990, ApJ, 349, 190

- Hartmann, L.W., Jones, B.F., Stauffer, J.R., & Kenyon, S.J., 1991, AJ, 101, 1050
- Hartmann, L., Soderblom, D.R., & Stauffer, J.R. 1987, AJ, 93, 907
- Herbig, G.H., Vrba, F.J., & Rydgren A.E., 1986, AJ, 91,575
- Herbig, G.H. 1998, ApJ, 497, 736
- Hillenbrand, L.H. 1997, AJ, 113, 1733
- Hunter, J. H. Jr. 1979, ApJ, 233, 946
- Hunter, J. H. Jr., & Fleck, R. C. 1982, ApJ, 256, 505
- Hunter, J. H. Jr., Sandford, M. T. II, Whitaker, R. W. & Klein, R. I. 1986. ApJ, 305, 309
- Jura, M. ApJ197, 575
- Kenyon, S.J., & Hartmann, L. 1995, ApJS, **101**, 117
- Kleiner, S. C., & Dickman, R., L. 1984. ApJ286, 255.
- Lawson, W.A., Feigelson, E.D., & Huenmoerder, D.P. 1996, MNRAS, 280, 1071
- Lee, C. W. & Myers, P. C. ApJ in press
- Leisawitz, D., Bash, F. N., & Thaddeus P. 1989. ApJS, 70, 731
- Lessieur, M. 1990. Turbulence in Fluids. Stochastic and Numerical Modeling. Kluwer Academic Publishers.
- Mac Low, M.-M.. 1999. ApJ, submitted
- Magnani, L., Blitz, L., & Mundy, L. 1985. ApJ, 295, 402
- Martin & Magazzu 1998. ASP Conf. Ser. 154, *The Tenth Cambridge Workshop on Cool Stars, Stellar Systems and the Sun*. Eds R. A. Donahue and J. A. Bookbinder, p. 1742
- Mizuno, A., Onishi, T., Yonekura, Y., Nagahama, T., Ogawa, H. & Fukui, Y. 1995. ApJ, 445, L161
- Moriarty-Schieven, G. H., Andersson, B-G., & Wannier, P. G. 1997. ApJ, 475, 642
- Mouschovias, T. Ch. 1991, in *The Physics of Star Formation and Early Stellar Evolution*, eds. C.J. Lada & N.D. Kylafis (Dordrecht: Kluwer) pp 61, 449
- Myers, P. C. & Khersonsky 1995. ApJ 442, 186
- Nakano, T. 1998. ApJ, 494, 587
- Neuhäuser, R., Sterzik, M. F., Torres, G., & Martín E. L. 1995. å, 299, L13
- Ostriker, E. C., Gammie, C. F., & Stone, J. M. 1998. ApJ, submitted
- Padoan, P., & Nordlund, A. 1999. ApJ, in press
- Palla, F., & Galli, D. 1997, ApJ, 476, L35
- Passot, T., Vázquez-Semadeni, E. & Pouquet, A. 1995. ApJ 455, 536 (PVP95)

- Raymond, Cox & Smith 1976. ApJ 204, 290
- Shu, F.H., Adams, F.C., & Lizano, S. 1987, ARA&A, 25, 23
- Sasao, T. 1973. PASJ, 25,1
- Siess, L., Forestini, M., & Bertout, C. 1997, A&A, 326, 1001
- Stauffer, J.R., Hartmann, L.W., & Barrado y Navascues, D. 1995, ApJ, 454, 910
- Swenson, F.J., Faulkner, J., Rogers, F.J., & Iglesias, C.A. 1994, ApJ, 425, 286
- Tohline, J. E., Bodenheimer, P. H., & Christodoulou, D. M. 1987. ApJ322, 787
- Ungerechts, H. & Thaddeus, P., 1987. ApJS, 63, 64
- Vázquez-Semadeni, E. Ballesteros-Paredes, J., & Rodríguez, L. F. 1997. ApJ 474, 292 (VBR97)
- Vázquez-Semadeni, E., Ostriker, E., Passot, T., Gammie, C. & Stone, J. 1999, in Protostars and Planets IV, eds. V. Mannings, A. Boss, S. Russell (Tucson: Univ. Of Arizona Press).
- Vázquez-Semadeni, Passot & Pouquet, 1995. ApJ 441, 702 (VPP95)
- Vázquez-Semadeni, E., Passot, T. & Pouquet, A. 1996. ApJ 473, 881 (VPP96)
- Walter, F.M., Brown, A., Mathieu, R.D., Myers, P.C., & Vrba, F.V., 1988, AJ, 96, 297
- Wichmann, R., Krautter, J., Schmitt, J.H.M.M., Neuhäuser, R., Alcalá, J.M., Zinnecker, H., Wagner, R.M., Mundt., R., & Sterzik, M.F., 1996, Å, 312, 439
- Williams, J. P., Blitz, L, & Stark, A. A. 1995. ApJ 451, 252



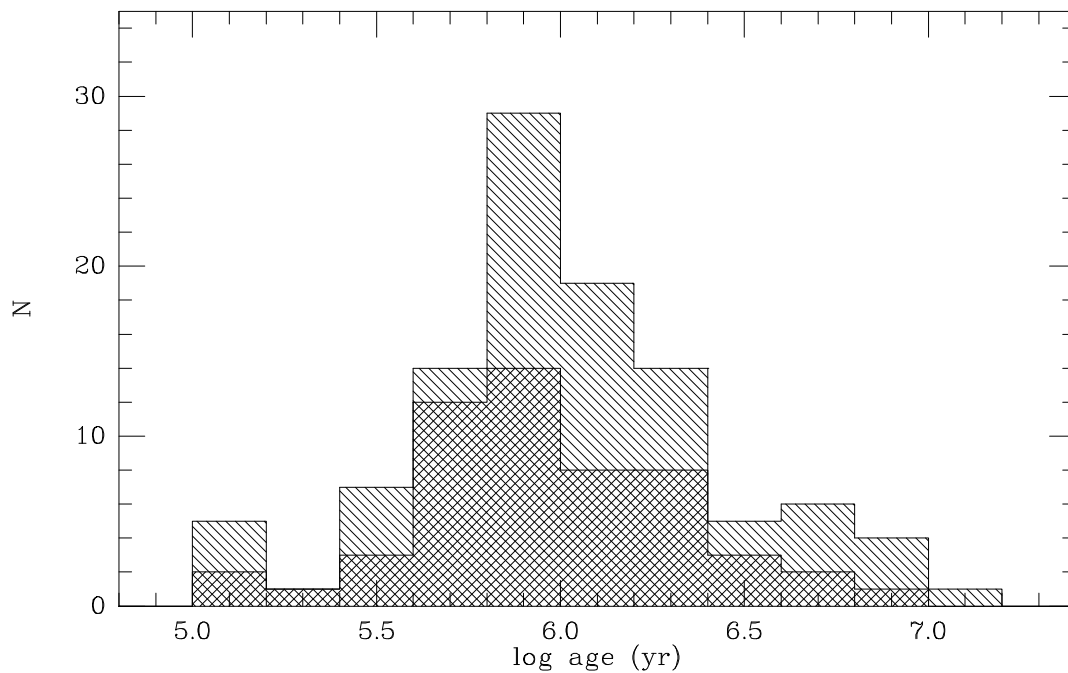


Fig. 1.— a) HR Diagram for stars in the Taurus-Auriga molecular cloud region, with evolutionary tracks from D’Antona & Mazzitelli (1994). Filled circles denote the Classical T Tauri Stars (CTTS). Open circles denote the Weak T Tauri Stars (WTTS). The great majority of stars have ages of ~ 1 Myr, and only a few stars have ages greater than ~ 3 Myr. The group of stars near the ~ 100 Myr isocrone were discovered with Einstein X-ray observations (Walter et al. 1988); X-ray detected sources in the region are generally older than 10 Myr (Briceño et al. 1997), and are likely to be field stars. b) Age histogram for the stars in fig 1a. Single line denotes the classical T-Tauri stars. Crossed lines, the weak T-Tauri stars. Note that the great majority of stars is between 1 and 3 Myr.

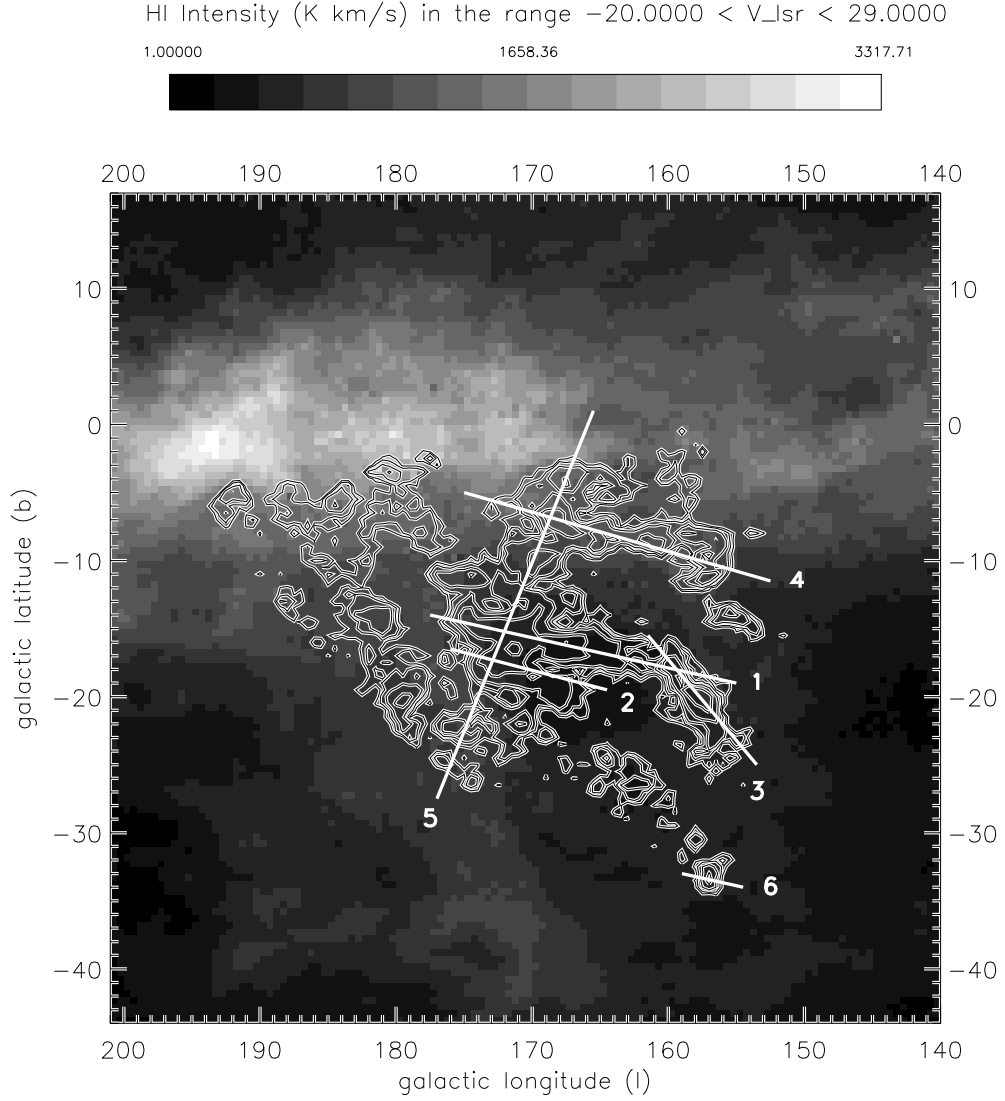
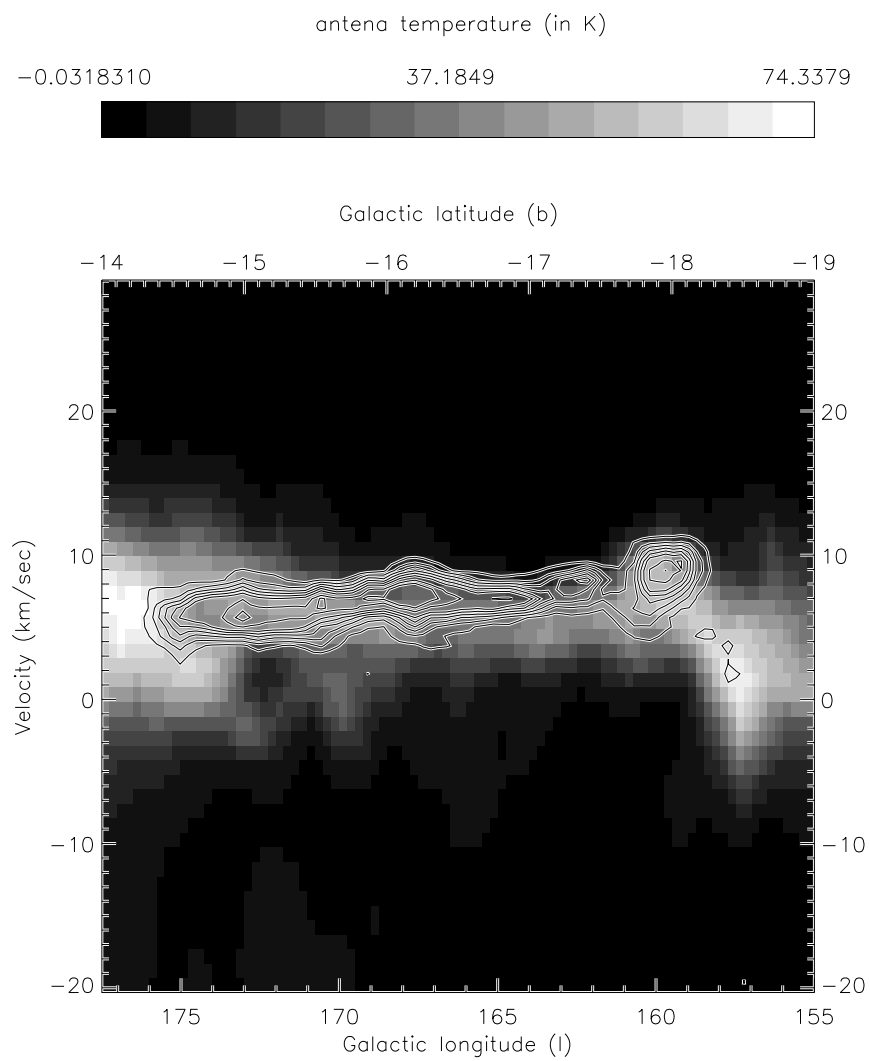
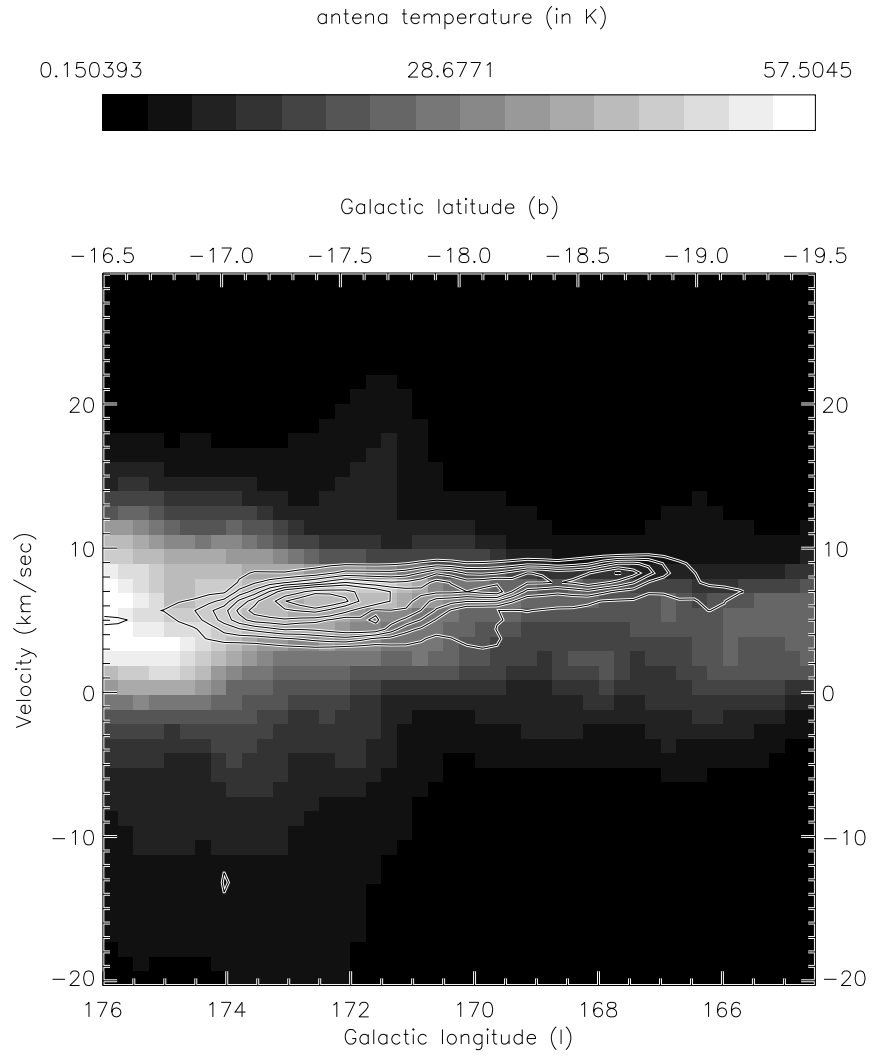
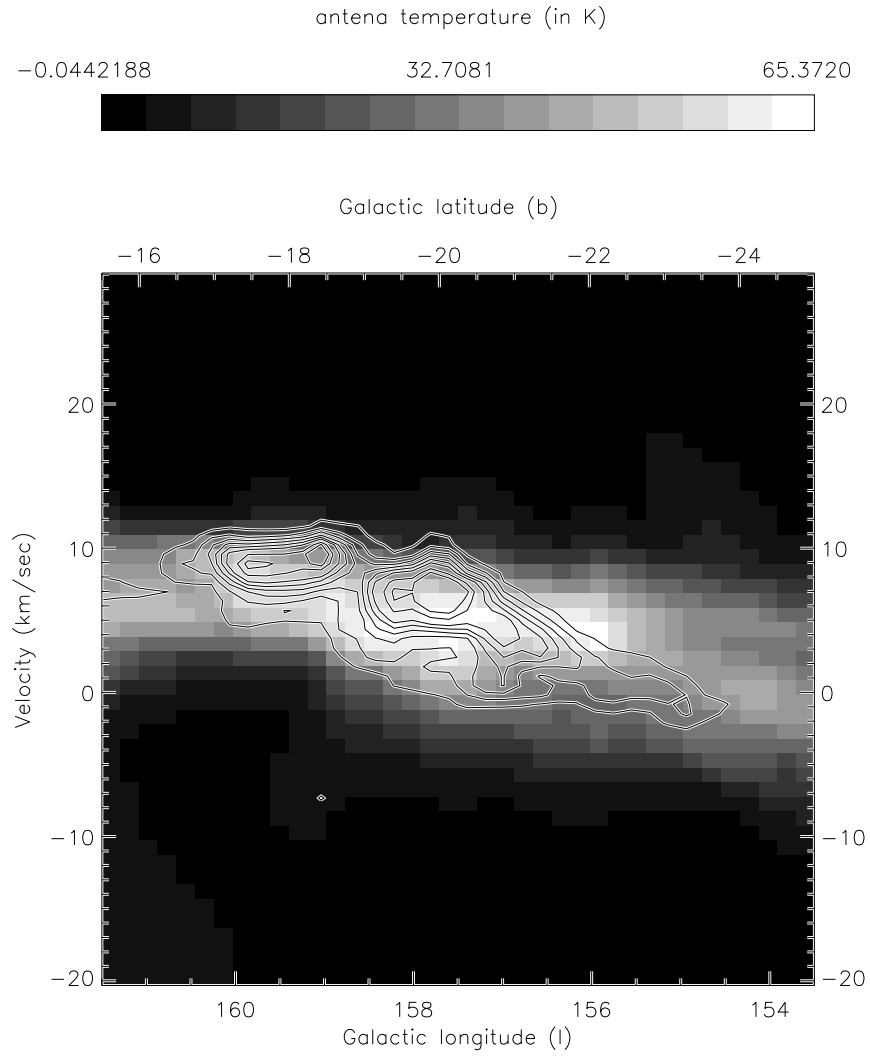
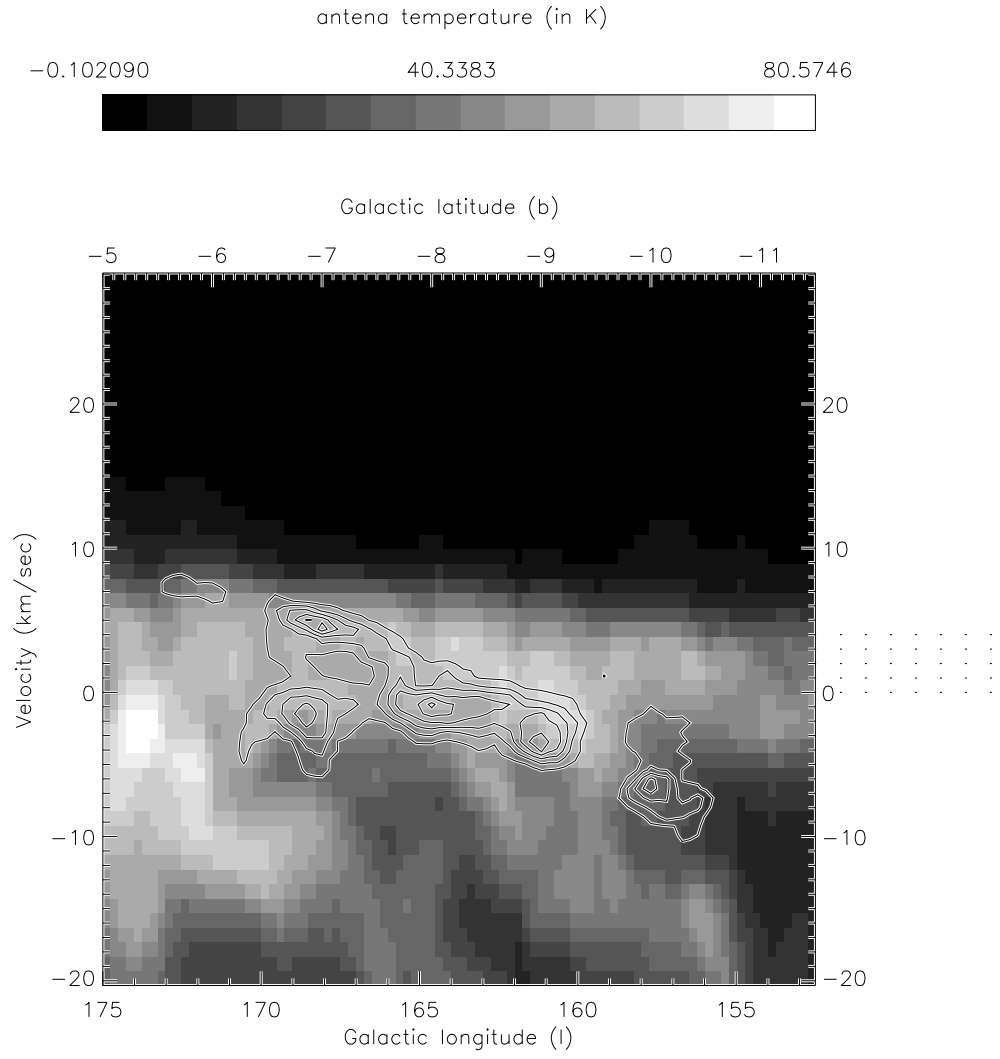


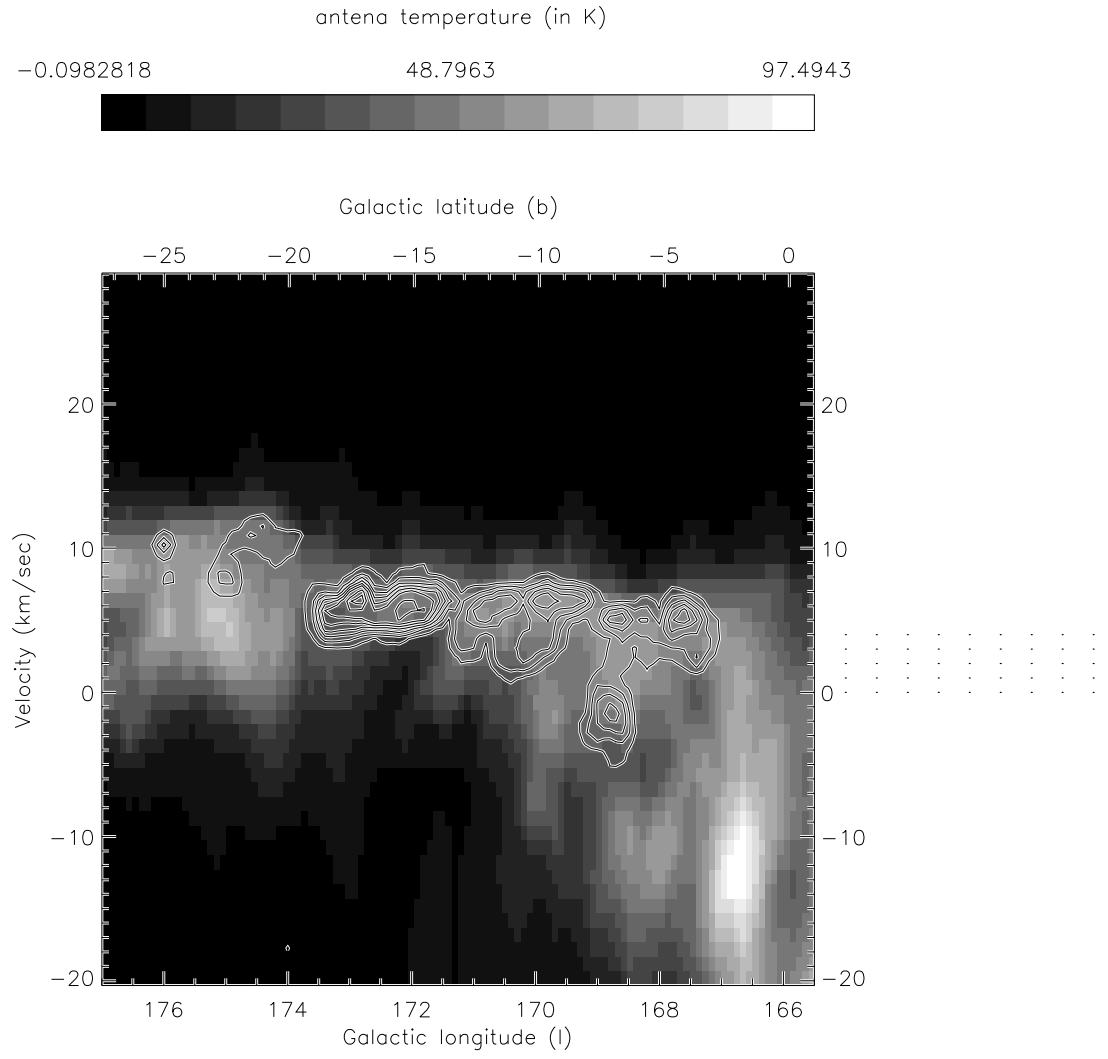
Fig. 2.— Velocity integrated (from -20.3 to 29.08 km s^{-1}) large-scale map of antenna temperature for CO (Ungerechts & Thaddeus 1987) and HI (Hartmann & Burton 1997) data through Taurus, in units of K km s^{-1} . Contours: 2, 4, 8, 16, 32, 64. The grey scale is indicated on the top. The white lines denote the places where the velocity-position diagrams have been made. (Lee: I have to include also the cut in L1457)











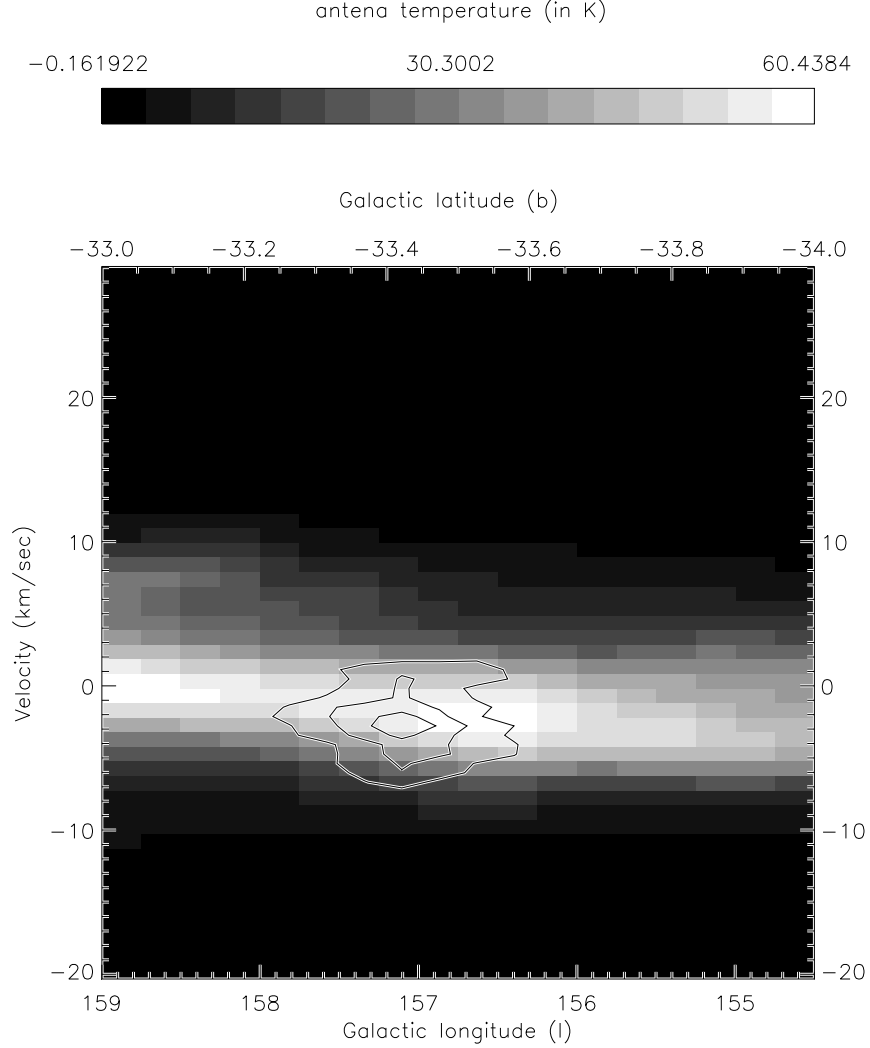


Fig. 3.— Velocity-Position diagrams at the positions showed in fig. 2. Grey scale denotes the HI emission, and contours denote the ^{12}CO emission. The y -axis denotes the velocity in km s^{-1} ; the upper x -axis denotes the galactic latitude, and the lower x -axis denotes the galactic longitude, both in degrees. Note the following general characteristics: a) wherever there is a ^{12}CO , HI is also found, with an approximate column density similar to that required by shielding. b) the converse is not true: not all HI in this velocity system is associated with molecular gas. c) at the same spatial position, the HI emission often does not peak at the same velocity than the ^{12}CO ; frequently there is a shift of a few km s^{-1} between the two species. d) velocity widths in the HI spectra are larger than the ^{12}CO spectra by a factor of roughly 3 or more. e) both the ^{12}CO and HI line profiles are asymmetric, as indicated by the variation of gray-scale and contours.

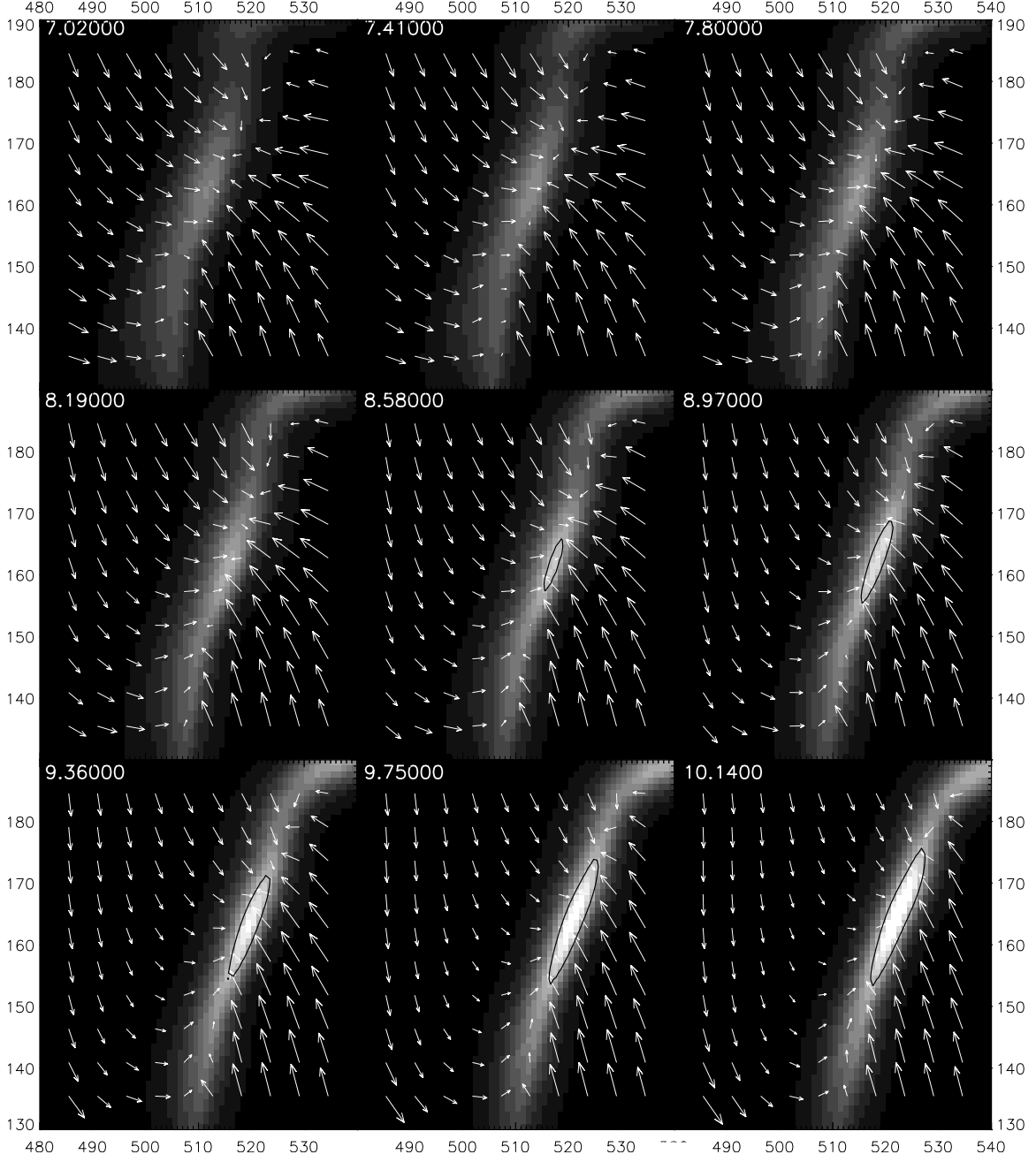


Fig. 4.— Time sequence of a small region of the simulation. We show the density field (grey scale), ranging from $\rho < 0.31 \text{ cm}^{-3}$ (darker) to $\rho > 56 \text{ cm}^{-3}$. The label in the upper left corner in each panel is the age in Myr after turning-off the star formation in the simulation. Note that material with $n > 35 \text{ cm}^{-3}$ (the “molecular cloud”) is formed in few Myr by the large-scale compression.

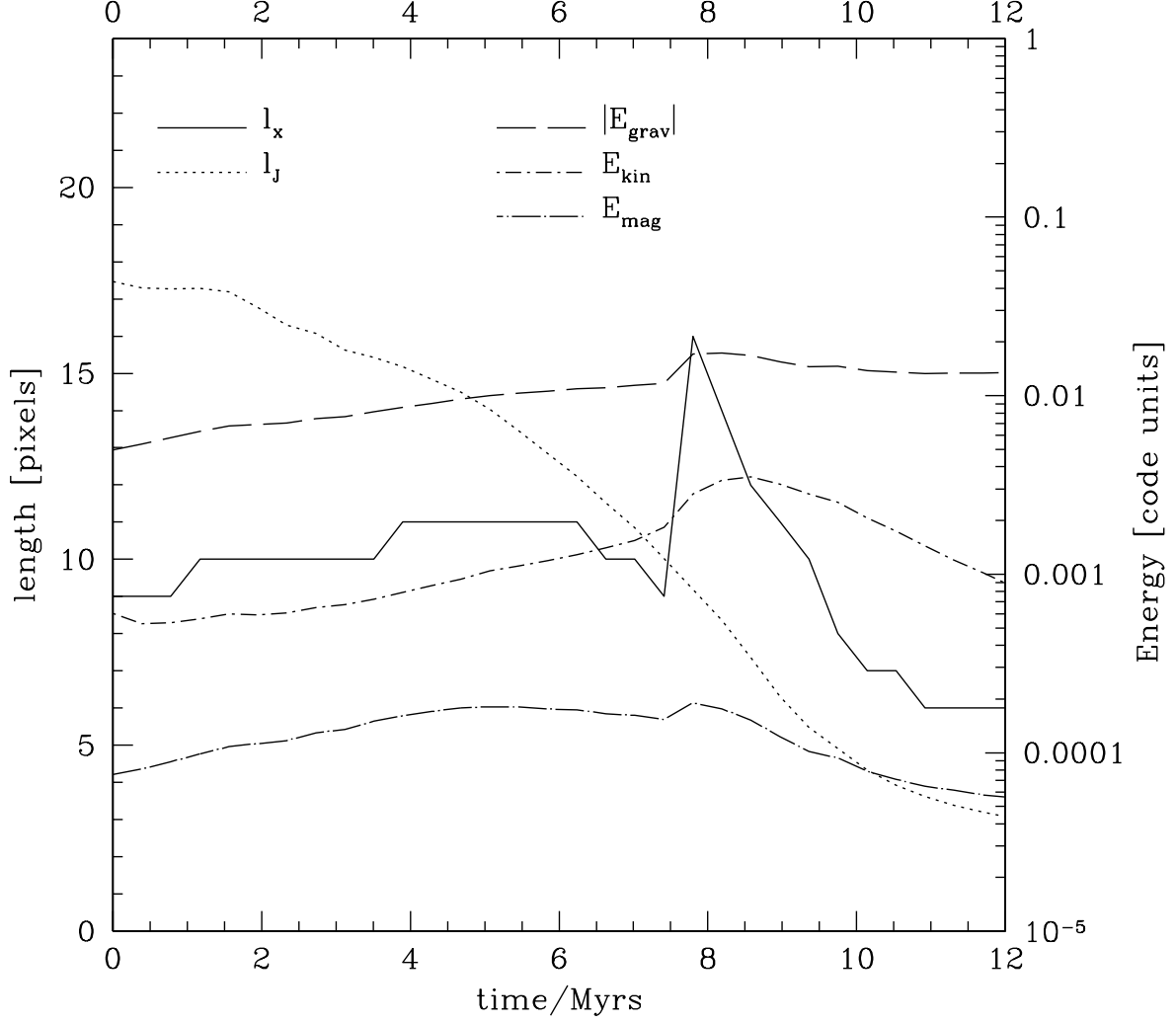


Fig. 5.— Time-evolution of the characteristic lengths (left-hand side of the y -axis), and energies (x -axis) for the region defined as a connected set of pixels with density equal or higher than $1/2$ value of the density maxima at each timestep. Solid line, l_x , the maximum length in the x -direction; dotted-line, l_J , the Jeans length as in eq. (1). Short-dashed line, absolute value of the gravitational energy; long-dashed line, kinetic energy in the frame of the cloud, and dotted-dashed line, magnetic energy. Note that initially the cloud is Jeans-stable, but after some time, it becomes Jeans-unstable. Also, note that the magnetic energy is two orders of magnitude lower than the gravitational energy, suggesting that there is no magnetic-flux problem, i.e., the cloud is supercriticall. The strong jump in the extensive quantities at $t \sim 8$ Myr. is due to the merging of the filament with another density feature, as can be seen in Fig. 4.

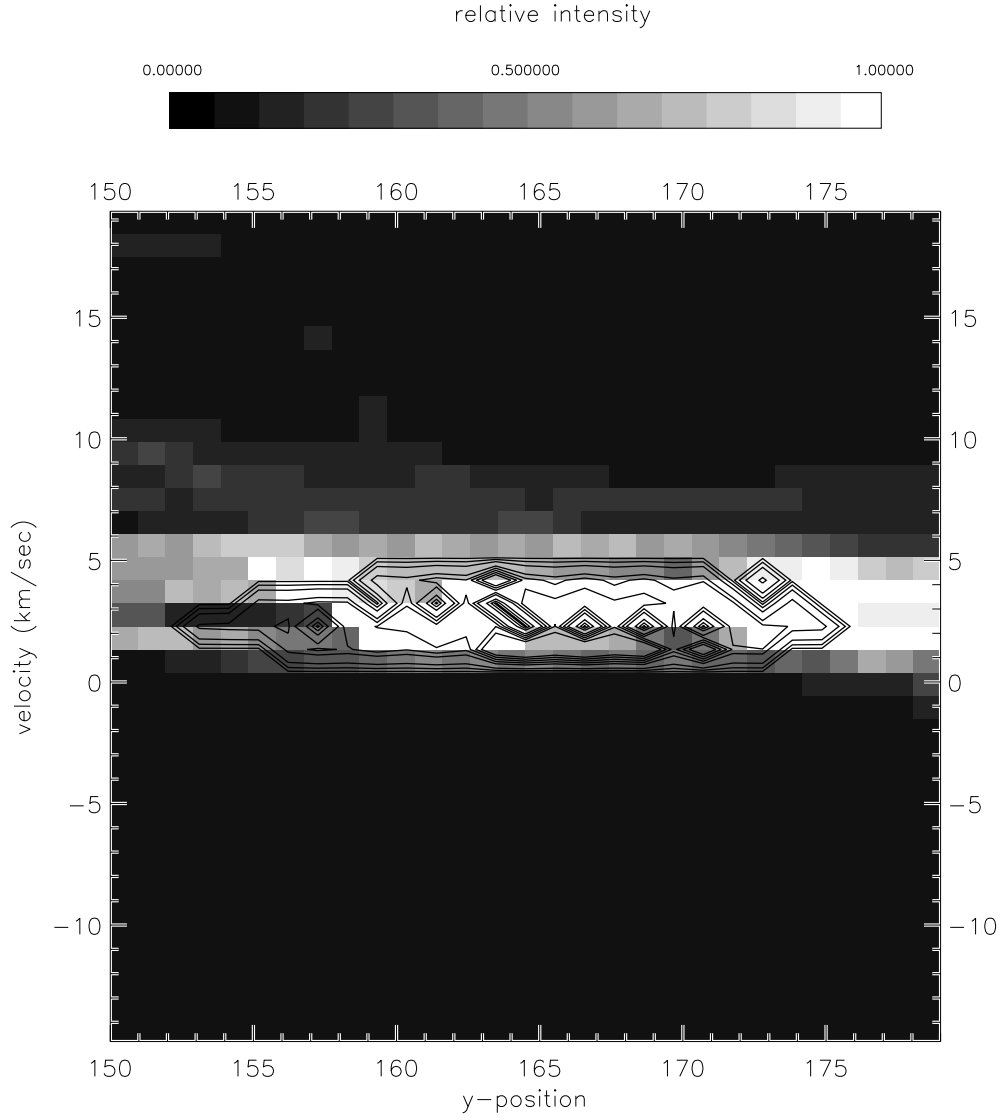


Fig. 6.— Synthetic Velocity-Position diagram for the cloud in panel 4i. As in fig. 3, grey scale denotes the “HI emission”, and contours denotes the “emission” coming from the “molecular cloud”. Note that the same characteristics observed in the observational position-velocity diagrams are reproduced also here.